Journal of Superconductivity and Novel Magnetism (2019) 32:3797–3802
https://doi.org/10.1007/s10948-019-05195-5

ORIGINAL PAPER

Effect of Trapped Magnetic Flux on Neutron Scattering in $La_{1.85}Sr_{0.15}CuO_4$ Superconductor

A. A. Bykov[1] · D. M. Gokhfeld[2] · E. V. Altynbaev[1] · K. Yu Terent'ev[2] · N. Martin[3] · S. V. Semenov[2] · S. V. Grigoriev[1,4]

Received: 15 April 2019 / Accepted: 20 June 2019 / Published online: 26 June 2019

Abstract
The superconducting $La_{1.85}Sr_{0.15}CuO_4$ ceramics has been studied by small angle neutron scattering, magnetization measurements, and scanning electron microscopy. Experiments have shown that the intensity of the magnetic scattering is 2–3 times higher in the field cooled regime than in the zero-field cooled regime. Additional magnetic heterogeneities due to closure of the trapped magnetic flux cause the excess scattering in the field cooled regime. The isotropic nature of the scattering is associated with the absence of a preferred direction of the Abrikosov vortices, which is caused by the random orientation of the ab planes of the anisotropic superconductor granules.

Keywords Superconductivity · SANS · Trapped field · LSCO ·

1 Introduction

The characteristics of the superconducting materials are strongly affected by the parameters of the pinning centers, which are located in these materials [1]. The method of the neutron depolarization on the superconducting heterogeneity [2, 3] is usually used to obtain information about the penetration of magnetic flux into a superconductor. In contrast to this method, small-angle neutron scattering (SANS) potentially can be used to directly observe pinning centers and obtain information about their size and distribution. Comparison of SANS, magnetic, and microstructural studies can provide a complete picture of the magnetic flux pinning in type-II superconductors.

Quite a lot of works are devoted to the study of single crystals superconductors by SANS [4–9]. In this case, Abrikosov vortices combine to a flux line lattice, which gives clear peaks on the scattering map [10, 11]. The results of the scattering experiments on the polycrystalline samples or ceramics are not so obviously clear, because the scattering intensity is low [12, 13]. But polycrystalline systems are very attractive for investigations due to their simplify synthesis.

At that point, experiments of scattering of polarized neutrons with taking into account magnetic-nuclear interference are especially interesting [14, 15]. These experiments make possible to separate the scattering contributions from the magnetic and nuclear structures. Consequently, information about a relation between the magnetic and nuclear structures also can be gotten. Unfortunately, the polarized neutron flux is currently unacceptably small for such weakly scattering systems as polycrystalline superconductors. The future solution is seen by the authors either in enhancing the scattering contrast, or in organizing a periodic scattering structure. This article is devoted to some interesting results which can be obtained now using the usual unpolarized neutron beam. An intensity of the unpolarized neutron beam is sufficient for a reliable experiment, which concerns a trapped magnetic flux. The trapped magnetic flux corresponds to the pinning potential of the system. Thermomagnetic prehistory is important for understanding of penetration of the magnetic flux into a superconductor. At the field cooled regime (FC), the magnetic flux penetrates into the whole sample before the start of measurements. At the zero-field cooled regime (ZFC), the sample has a transition to the superconducting state without the external magnetic field, and the magnetic flux penetrates during measurements. At both regimes, the density of the trapped magnetic flux usually

✉ A. A. Bykov
redi87@bk.ru

[1] NRC Kurchatov Institute – PNPI, Gatchina, Russia 188300

[2] Federal Research Center KSC SB RAS, Kirensky Institute of Physics, Krasnoyarsk, Russia 660036

[3] Laboratoire Léon Brillouin, CEA, CNRS, Université Paris-Saclay, CEA Saclay, 91191 Gif-sur-Yvette, France

[4] Saint-Petersburg State University, Ulyanovskaya 1, Saint-Petersburg, Russia 198504

depends on the number of pinning centers. In the present paper, the results of a study of the trapped field in $La_{1.85}Sr_{0.15}CuO_4$ (LSCO) superconducting ceramics by the SANS are given.

2 Materials and Methods

Polycrystalline $La_{1.85}Sr_{0.15}CuO_4$ with the critical temperature $T_c = 37.7$ K was synthesized by the standard solid phase sintering technique in Kirensky Institute of Physics. Scanning electron microscopy was performed on microscope Hitachi TM 3000. Magnetization curves $M(H)$ were measured by using QD PPMS-6000 magnetometer. The sample had the parallelepiped form with the size of about $0.5 \times 5 \times 10$ mm^3 and mass of about 21 mg.

The SANS experiment was carried out on the PA-20 small angle machine of the Orphée reactor in Saclay CEA-CNRS Laboratory Leon Brillouin [16]. PA20 is installed at the end of the cold neutron guide; the wavelength of the incoming neutrons is produced from a white beam by a mechanical velocity selector. The neutrons are then collimated by a series diaphragms and sections of moveable guides in an evacuated collimator. The sample holder was equipped with a double goniometer, height, and translation motions of a rotating table that host cryomagnet and helium cryostat. In neutron measurements, the external magnetic field was directed along an unpolarized neutron beam with a wavelength $\lambda = 5.5$ Å. The ^{3}He multi-detector, with 128×128 cells of 5×5 mm^2, was positioned at 18 m distance from the sample in the longitudinal direction in its vacuum tube.

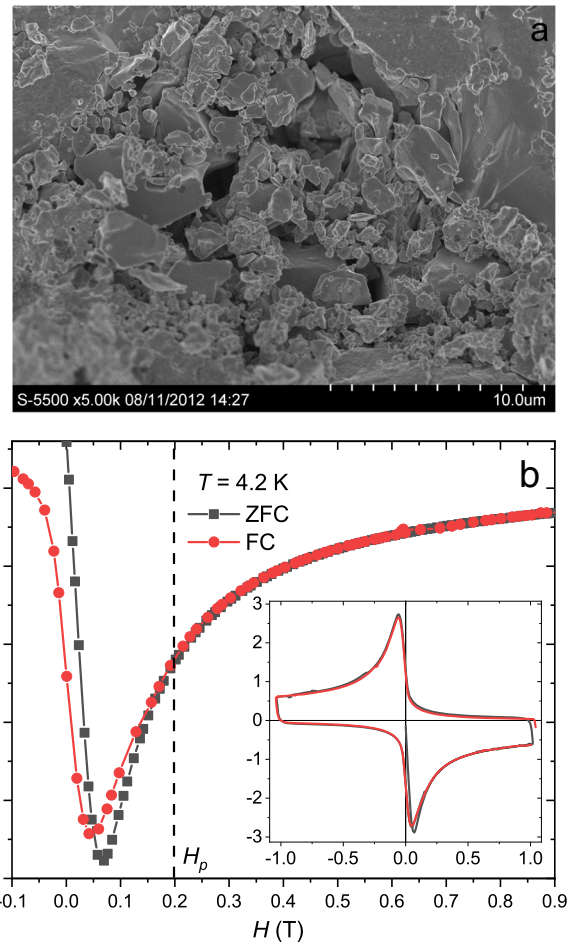

Fig. 1 Typical microphotograph of the sample (**a**), the dependence of the magnetization versus the external magnetic field (**b**). The inset shows a complete magnetization hysteresis loop

3 Results and Discussions

Figure 1 a shows a microphotograph of the sample. The sample consists of sintered granules with sizes from 100 nm to several micrometers. The magnetization hysteresis loop at $T = 4.2$ K is presented in Fig. 1b. Such magnetization curves are typical for type-II superconductors: the behavior of the magnetization hysteresis loop is determined by an entrance of Abrikosov vortices into the sample (as the external magnetic field H increases) and by a trap of the magnetic flux (as H decreases). The magnetic flux penetrates into the intergranular space of the ceramic sample even at H less than 0.01 T [17]. But penetration into the superconducting granules starts at higher fields $\mu_0 H \sim 0.01$–0.02 T. The initial magnetization branch (ZFC at Fig. 1b) begins to coincide with the full hysteresis loop (FC) at $\mu_0 H \approx 0.2$ T, which corresponds to a full penetration field H_p. At $H = H_p$, the vortices penetrated into whole volume of the sample [18]. At the fields above H_p, the concentration of Abrikosov vortices in the sample increases with H. The magnetic flux density in the sample is higher during decrease of H than at the same value of increasing H. This is due to the pinning of Abrikosov vortices and results in the hysteresis on the magnetization curve.

Figure 2 shows the dependence of an integrated intensity I on a momentum transfer Q obtained by radial averaging of the SANS map at $T = 60$ K. This temperature is significantly higher than the T_c so that the observed scattering is purely of nuclear origin. A fit of the experimental data is also shown in accordance with the Beaucage model [19]:

$$I(Q) = G \cdot \exp\left(-\frac{Q^2 R_g^2}{3}\right) + B \cdot \left[\frac{\left(\operatorname{erf}\left\{Q\frac{R_g}{\sqrt{6}}\right\}\right)^3}{Q}\right]^p,$$

where R_g is the radius of gyration of the granules, G is an exponential prefactor, B is a constant prefactor, and p is a parameter defined by a scattering type. There is a high Q region, which is corresponded to the Porod law. It indicates a sharp border of the ceramic granules. In the region of small $Q < 0.01$ Å^{-1}, the Porod law ($p = 4$) is not satisfied and one can only estimate the size of scattering centers using the

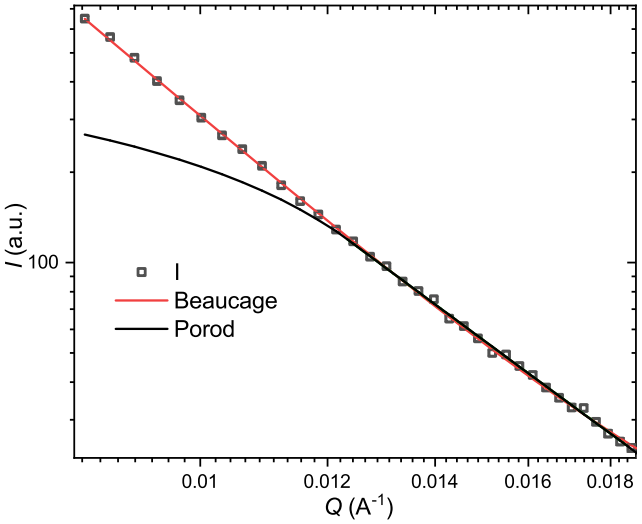

Fig. 2 Momentum transfer dependence of the integrated intensity of the nuclear part of scattering at $T = 60$ K

Guinier law. We take the shape of granules as a sphere for simplicity and obtain a diameter of granules about 250 nm from the radius of gyration. This value is close to the size of the granules in the microphotographs.

At $T < T_c$, the scattering is a mixture of the magnetic and nuclear contributions. The intensity measured at $T = 60$ K, where there is only nuclear scattering, was subtracted from the total intensity to obtain the magnetic part of the scattering. Figure 3 a shows a typical map of the magnetic part of the small-angle scattering. The neutron scattering occurs only if the scattering vector is perpendicular to the magnetic moment of the scattering region. The observed scattering is equally distributed over all azimuthal angles of the SANS map. The isotropic distribution indicates the magnetic moments for magnetic heterogeneity are randomly oriented in the sample.

The figure also shows the radial averaging scheme. The scattering data were averaged along the radius of the white circle on the SANS map. The dependencies of the scattering intensity versus momentum transfer obtained by this radial averaging are presented in Fig. 3b. It can be seen that the scattering intensity depends on the cooling regime.

Figure 4 shows the dependencies of the integrated intensity on the applied magnetic field at different temperatures. Small negative intensity values near zero can be associated with insufficient background measurement statistics. The intensity increases with increasing magnetic field up to H_p ($\mu_0 H_p \approx 0.2$ T at 5 K and $\mu_0 H_p \approx 0.15$ T at $T = 15$ K). This increase is caused by an increasing of the number of magnetic heterogeneities in the sample.

The intensity of the magnetic scattering of unpolarized neutrons for structures without long-range order is proportional to the number of magnetic irregularities and to the magnetic contrast $\Delta\rho_{mag}$ between the magnetic irregularity and the containing matrix.

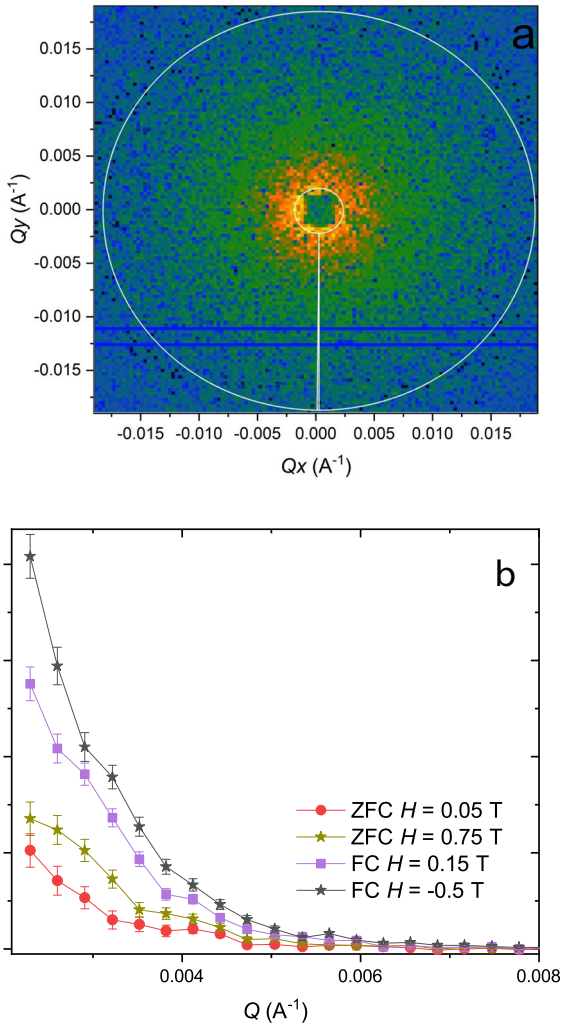

Fig. 3 A typical map of the magnetic part of the scattering at $\mu_0 H = -0.3$ T in the FC regime (**a**) and the momentum transfer dependencies of the radially averaged magnetic scattering (**b**)

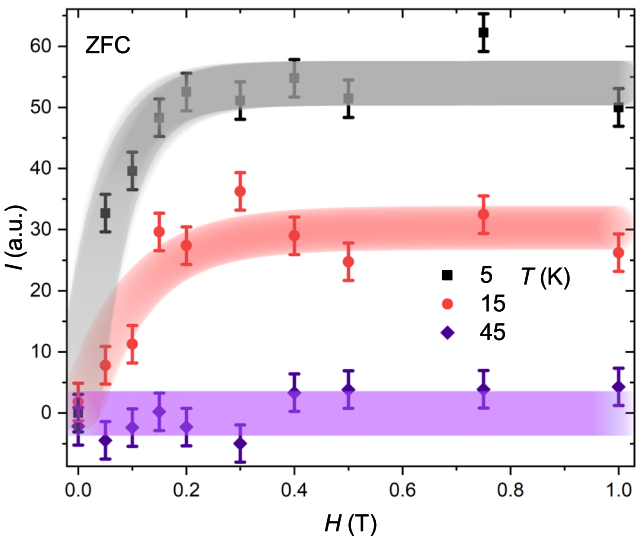

Fig. 4 Integral intensity versus the applied magnetic field at the ZFC regime and different temperatures

$$I(Q) = a{\cdot}\Delta\rho_{mag}^2 \, N \, V^2{\cdot}\left[\langle F^2(Q)\rangle - \langle F(Q)\rangle^2{\cdot}\{1 - S_{int}(Q)\}\right],$$

where a is a scaling constant, N is the number of scattering centers, V is the characteristic volume of the magnetic irregularities, $F(Q)$ is the form factor, and $S_{int}(Q)$ is an interference function taking into account the local correlation between magnetic irregularities ($S_{int}(Q) = 1$ for a random distribution). The magnetic irregularities have borders where local magnetic field jumps. In our case, the magnetic irregularities are Abrikosov vortices and the magnetic flux passing through the intergranular boundaries. The matrix is the superconductor volume free from magnetic field.

In small external magnetic fields, the sample excludes the magnetic flux, so there is no magnetic heterogeneity inside the sample. An increase of the magnetic field leads to the penetration of Abrikosov vortices into the sample. At $H > H_p$, the scattering intensity practically does not increase. Also, as one can see, the intensity values decreases as the temperature increases. An increase of temperature leads to increase in the magnetic penetration depth; therefore, the contrast of the irregularities and the corresponding intensity of the scattering decrease. At temperatures higher than T_c ($T = 45$ K in the figure), the intensity is equal to zero within the error. This means that the magnetic field completely penetrates into the sample, and the magnetic heterogeneity and scattering disappear.

Figure 5 shows the dependencies of the integrated intensity on the applied magnetic field in various modes of sample cooling. Temperature and magnetic field were changed during the experiment as follows: firstly, the sample was cooled till $T = 5$ K at zero external magnetic field. After that, the magnetic field was applied and SANS measurements were carried out (ZFC mode). When the field value reached $\mu_0 H = 1$ T, the system was heated to 60 K. Then the temperature was again dropped to $T = 5$ K in the external magnetic field $\mu_0 H = 1$ T (FC mode). Further, the magnetic field was decreased from 1 to − 1 T and then increased to 1 T again. In Fig. 5, the temperature changes are shown by arrows.

At $H > H_p$, the scattering intensity is mostly determined by the number of defects: this situation is observed at ZFC regime. At $H = H_p$, the vortices reach the central regions of the granules, and the number of scattering irregularities saturates. Consequently, the growth of the $I(H)$ dependence stops too. At the FC regime, the intensity values approximately correspond to the values in ZFC mode at the $\mu_0 H = 1$ T. But when the magnetic field decreases from 1 T to 0, the intensity values increase in 2–3 times. When the field returns from negative to positive values, the intensity decreases only in 1.2 times, but not to the values of ZFC regime.

The observed change in the intensity can be related to a change of the effective magnetic field into the intergranular space at ZFC and FC regimes. The lines of the magnetic induction generated by the currents circulating in the granules are closed into the intergranular space. These lines are co-directed with the external magnetic field at the ZFC regime and opposite to the external field at the FC regime [20]. At the FC regime, opposite direction of the magnetic flux into the intergranular space appears and additional magnetic heterogeneity may occur, as shown in the inset of Fig. 5. The inset shows that a granule at the FC mode has 4 magnetic boundaries, where the direction of magnetic induction changes. There are only two such magnetic irregularities for a granule at ZFC mode. Thus, the additional magnetic irregularities lead to the increasing intensity with the decreasing external magnetic field. With a further change of the external magnetic field from − 1 to 1 T, the value of the contrast is kept, while the sample traps the magnetic flux. At FC regime, a slight decrease of the intensity is observed at high fields. This can be attributed to suppression of superconductivity by the magnetic field and corresponding decrease of the magnetic heterogeneity. We expect the disappearance of scattering at magnetic fields close to the upper critical field H_{c2}. The additional

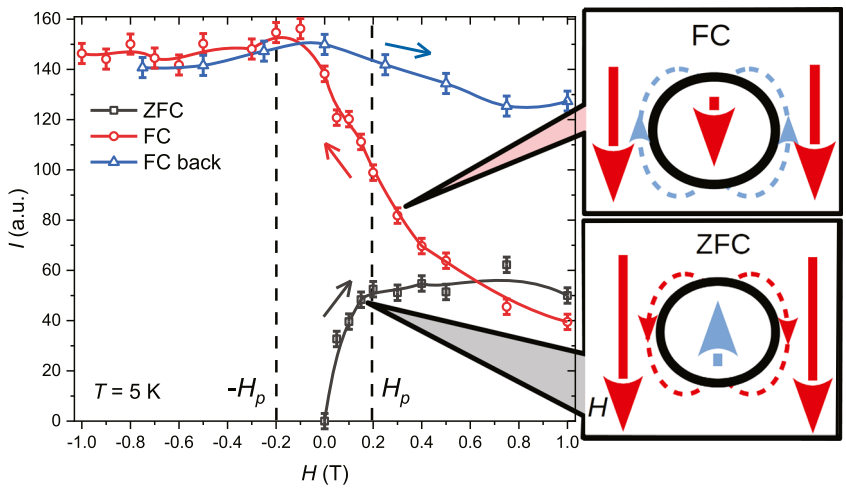

Fig. 5 Integral intensities versus the applied magnetic field for various cooling modes. The inset shows the schemes of the appearance of the additional magnetic heterogeneity

magnetic irregularities correlate well with a fact that the field is trapped in the type-II superconductors in a form of "inverse" domains (of the superconducting state in a normal state matrix). Such domains were observed using Faraday effect [21–23]. A pair of the "inverse" domains have oppositely directed magnetization and separate by an "annihilation" zone. That "annihilation" zone seems to be the additional inhomogeneity, which is origin of additional neutron scattering.

The isotropic nature of the scattering on the SANS maps can also be explained by the trapped magnetic flux in the sample. The direction of the Abrikosov vortices of the anisotropic granules can differ from the direction of the external field. It is known [24, 25] that the flow of supercurrent occurs predominantly in the *ab* planes of anisotropic superconducting granules. The Abrikosov vortices enter into anisotropic granules perpendicular to the *ab* planes. For ceramic samples, granules have an irregular shape and are randomly oriented. Due to the fact that any directions of the magnetic moments of the irregularities are possible, scattering occurs in all directions.

4 Conclusions

In conclusion, although the LCSO superconductor does not have sufficient contrast for the study by polarized neutrons, magnetic scattering is still quite significant and suitable for unpolarized neutron fluxes. The study of the LSCO superconducting ceramic by the SANS method showed a significant dependence of the scattering on the thermomagnetic prehistory of the sample. When a magnetic flux is trapped into the sample, the scattering increased by a factor of 2–3, which is due to the induced magnetic heterogeneity into the sample. Precious information about the initial stage of the penetration of a magnetic field into a superconductor can be obtained by SANS below the first critical field of a superconductor.

Acknowledgments The authors are grateful to G.P. Kopitsa and V.V. Runov for fruitful discussions.

Funding Information The work is supported by the Russian Science Foundation (project No. 17-72-10067).

References

1. Brandt, E.H.: The flux-line lattice in superconductors. Reports Prog. Phys. **58**, 1465–1594 (1995). https://doi.org/10.1088/0034-4885/58/11/003
2. Roest, W., Rekveldt, M.T.: Three-dimensional neutron-depolarization analysis of the magnetic flux distribution in $YBa_2Cu_3O_7$. Phys. Rev. B. **48**, 6420–6425 (1993). https://doi.org/10.1103/PhysRevB.48.6420
3. Dmitriev, R.P., Jagood, R.Z., Zhuchenko, N.K., Volkov, M.P., Leyarovski, E.I.: A study of the mixed state of the $YBa_2Cu_3O_{6.9}$ superconducting ceramics by neutron depolarization. Zeitschrift fur Phys. B Condens. Matter. **83**, 155–159 (1991). https://doi.org/10.1007/BF01309411
4. Chang, J., White, J.S., Laver, M., Bowell, C.J., Brown, S.P., Holmes, A.T., Maechler, L., Strässle, S., Gilardi, R., Gerber, S., Kurosawa, T., Momono, N., Oda, M., Ido, M., Lipscombe, O.J., Hayden, S.M., Dewhurst, C.D., Vavrin, R., Gavilano, J., Kohlbrecher, J., Forgan, E.M., Mesot, J.: Spin density wave induced disordering of the vortex lattice in superconducting $La_{2-x}Sr_xCuO_4$. Phys. Rev. B. **85**, 134520 (2012). https://doi.org/10.1103/PhysRevB.85.134520
5. Gilardi, R., Mesot, J., Drew, A., Divakar, U., Lee, S.L., Forgan, E.M., Zaharko, O., Conder, K., Aswal, V.K., Dewhurst, C.D., Cubitt, R., Momono, N., Oda, M.: Direct evidence for an intrinsic square vortex lattice in the overdoped high-Tc superconductor $La_{1.83}Sr_{0.17}CuO_{4+\delta}$. Phys. Rev. Lett. **88**, 217003 (2002). https://doi.org/10.1103/PhysRevLett.88.217003
6. Li, Y., Egetenmeyer, N., Gavilano, J.L., Barišić, N., Greven, M.: Magnetic vortex lattice in $HgBa_2CuO_4$ observed by small-angle neutron scattering. Phys. Rev. B. **83**, 054507 (2011). https://doi.org/10.1103/PhysRevB.83.054507
7. Brown, S.P., Charalambous, D., Jones, E.C., Forgan, E.M., Kealey, P.G., Erb, A., Kohlbrecher, J.: Triangular to square flux lattice phase transition in $YBa_2Cu_3O_7$. Phys. Rev. Lett. **92**(067004), (2004). https://doi.org/10.1103/PhysRevLett.92.067004
8. White, J.S., Hinkov, V., Heslop, R.W., Lycett, R.J., Forgan, E.M., Bowell, C., Strässle, S., Abrahamsen, A.B., Laver, M., Dewhurst, C.D., Kohlbrecher, J., Gavilano, J.L., Mesot, J., Keimer, B., Erb, A.: Fermi surface and order parameter driven vortex lattice structure transitions in twin-free $YBa_2Cu_3O_7$. Phys. Rev. Lett. **102**(097001), (2009). https://doi.org/10.1103/PhysRevLett.102.097001
9. Eskildsen, M.R., Forgan, E.M., Kawano-Furukawa, H.: Vortex structures, penetration depth and pairing in iron-based superconductors studied by small-angle neutron scattering. Reports Prog. Phys. **74**, 124504 (2011). https://doi.org/10.1088/0034-4885/74/12/124504
10. Chang, J.J., Mesot, J.: Microscopic neutron investigation of the Abrikosov state of high-temperature superconductors. Pramana - J. Phys. **71**, 679–685 (2008). https://doi.org/10.1007/s12043-008-0256-0
11. Delamare, M.P., Poullain, G., Simon, C., Sanfilippo, S., Chaud, X., Brûlet, A.: Vortex lattice accommodation on twin boundaries in $YBa_2Cu_3O_7$ studied by neutron diffraction. Eur. Phys. J. B. **6**, 33–38 (1998). https://doi.org/10.1007/s100510050523
12. Papoular, R.J., Collin, G.: Polarized-neutron study of the $YBa_2Cu_3O_7$ system: granular versus bulk superconductivity. Phys. Rev. B. **38**, 768–771 (1988). https://doi.org/10.1103/PhysRevB.38.768
13. Kopitsa, G.P., Runov, V.V., Okorokov, A.I., Lyubutin, I.S., Frolov, K.V.: Small-angle polarized neutron scattering in $YBa_2(Cu_{0.9}Fe_{0.1})_3O_{7-y}$ ceramics at T =290-550 K. Appl. Phys. A Mater. Sci. Process. **74**, s628–s630 (2003). https://doi.org/10.1007/s003390201618
14. Kopitsa, G.P., Runov, V.V., Okorokov, A.I.: Spin correlations in $YBa_2(Cu_{1-x}F_x)_3O_{7+y}$ ceramic. Phys. Solid State. **40**, 19–22 (1998). https://doi.org/10.1134/1.1130223
15. Gordeyev, G., Okorokov, A., Runov, V., Runova, M., Toperverg, B., Brulet, A., Kahn, R., Papoular, R., Rossat-Mignod, J., Glattli, H., Eckerlebe, H., Kampmann, R., Wagner, R.: Small-angle scattering of polarized neutrons in HTSC ceramics. Phys. B Condens. Matter. **234–236**, 837–838 (1997). https://doi.org/10.1016/S0921-4526(96)01115-5
16. Chaboussant, G., Désert, S., Lavie, P., Brûlet, A.: PA20 : a new SANS and GISANS project for soft matter, materials and magnetism. J. Phys. Conf. Ser. **340**, 012002 (2012). https://doi.org/10.1088/1742-6596/340/1/012002

17. Landau, I.L., Willems, J.B., Hulliger, J.: Detailed magnetization study of superconducting properties of $YBa_2Cu_3O_{7-x}$ ceramic spheres. J. Phys. Condens. Matter. **20**, 095222 (2008). https://doi.org/10.1088/0953-8984/20/9/095222
18. Gokhfeld, D.: Critical current density and trapped field in HTS with asymmetric magnetization loops. J. Phys. Conf. Ser. **695**, 012008 (2016). https://doi.org/10.1088/1742-6596/695/1/012008
19. Beaucage, G.: Approximations leading to a unified exponential/power-law approach to small-angle scattering. J. Appl. Crystallogr. **28**, 717–728 (2002). https://doi.org/10.1107/s0021889895005292
20. Balaev, D.A., Popkov, S.I., Semenov, S.V., Bykov, A.A., Shaykhutdinov, K.A., Gokhfeld, D.M., Petrov, M.I.: Magnetoresistance hysteresis of bulk textured $Bi_{1.8}Pb_{0.3}Sr_{1.9}Ca_2Cu_3O_x$ + Ag ceramics and its anisotropy. Phys. C Supercond. its Appl. **470**, 61–67 (2010). https://doi.org/10.1016/j.physc.2009.10.007
21. Schuster, T., Koblischka, M.R., Moser, N., Kronmüller, H.: Observation of nucleation and annihilation of flux-lines with opposite sign in high-Tc superconductors. Phys. C Supercond. **179**, 269–278 (1991). https://doi.org/10.1016/0921-4534(91)92171-7
22. Schuster, T., Koblischka, M.R., Ludescher, B., Kronmüller, H.: Observation of inverse domains in high T c superconductors. J. Appl. Phys. **72**, 1478–1485 (1992). https://doi.org/10.1063/1.351712
23. Potratz, R., Klein, W., Habermeier, H.U., Kronmüller, H.: The determination of flux density gradients in Nb_3Sn diffusion layers by means of the magneto-optical faraday effect. Phys. Status Solidi. **60**, 417–426 (1980). https://doi.org/10.1002/pssa.2210600211
24. Bugoslavsky, Y.V., Kovalsky, V.A., Minakov, A.A., Kojima, H., Tanaka, I.: Orientation of the flux line lattice in anisotropic superconductors. J. Magn. Magn. Mater. **157–158**, 671–672 (1996). https://doi.org/10.1016/0304-8853(95)00960-4
25. Gokhfel'd, D.M., Balaev, D.A., Semenov, S.V., Petrov, M.I.: Magnetoresistance anisotropy and scaling in textured high-temperature superconductor Bi1.8Pb0.3Sr1.9Ca2Cu3O x. Phys. Solid State. **57**, 2145–2150 (2015). https://doi.org/10.1134/S1063783415110128